38th Fluid Dynamics Conference and Exhibit, 23–26 June 2008, Seattle, Washington

Effect of Freestream Noise on Roughness-Induced Transition at Mach 6

Katya M. Casper* and Brad M. Wheaton*

School of Aeronautics and Astronautics, Purdue University, West Lafayette, IN 47907-1282

Heath B. Johnson†

Department of Aerospace Engineering and Mechanics, University of Minnesota, Minneapolis, MN, 55455

Steven P. Schneider‡

School of Aeronautics and Astronautics, Purdue University, West Lafayette, IN 47907-1282

The effects of freestream noise on roughness-induced transition were measured for the HIFiRE forecone model. Temperature-sensitive paint measurements were used to visualize the wake of the roughness elements under quiet and noisy flow. The transition Reynolds number increased under quiet flow, for a less-than-effective trip, by a factor of up to 6.4 when referenced to the trip location. The difference in transition location between quiet and noisy flow conditions is significantly reduced when effective trips are used, but quiet flow still delays the transition location for an effective trip. STABL calculations of the flow over the model at 0 and 6° angle of attack were used to quantify the results.

The effect of an isolated roughness on the nozzle wall of the BAM6QT is also being studied. The nozzle wall features a thick laminar boundary layer, allowing measurements of the growth of instabilities. Temperature-sensitive paint measurements of the wake behind an isolated roughness element were obtained. In quiet flow, several hot streaks are visible.

Nomenclature

AoA	angle of attack
k	roughness height (in)
P_0	tunnel stagnation pressure
$P_{0,i}$	initial tunnel stagnation pressure
T_0	tunnel stagnation temperature
t	time into run (s)
Re/ft	unit Reynolds number (1/ft)
Re_k	Reynolds number based on roughness height k and local conditions in the undisturbed boundary layer at the height k
Re_{xk}	Reynolds number based on trip location and edge conditions at the trip
Re_{xtr}	Reynolds number based on transition location and edge conditions at the transition location
x_{tr}	axial transition onset location (from nose)
z	axial tunnel coordinate measured from throat
δ	boundary-layer thickness (in)
δ^*	boundary-layer displacement thickness (in)

I. Introduction

Laminar-turbulent transition is important for reentry vehicles but can be difficult to predict. When a boundary layer transitions to turbulence, parameters including heat transfer and skin friction are affected. This can impact the thermal protection system, the glide distance for long-range hypersonic vehicles, and other design parameters. One factor affecting transition is surface roughness, whether it is an intentional

*Research Assistant, Student Member AIAA

†Senior Research Associate, Senior Member AIAA

‡Professor, Associate Fellow AIAA

part of the vehicle design or an artifact of the vehicle's construction. Understanding the effect of roughness on transition and being able to predict where transition will occur when roughness is present is a major thrust of current hypersonic research.

Many studies have been conducted on roughness effects on transition. Schneider[1] reviewed roughness-induced transition, stating "the effect of roughness on hypersonic boundary-layer transition has been studied for three primary purposes: to trip a laminar layer to turbulence, to determine whether naturally occurring roughness is expected to cause early transition, and to determine the largest allowable roughness that will not affect the location of transition." Most of this research was conducted in conventional tunnels which have high noise levels near 1% and sometimes as high as 2-3% of the mean. These high noise levels can cause transition much earlier than in flight.[2,3,4] Only a few studies have looked at the effect of noise on roughness-induced transition.[5,6,7] Several of these studies have been conducted in the Boeing/AFOSR Mach-6 Quiet Tunnel (BAM6QT). The BAM6QT is the only operational hypersonic quiet tunnel in the world. It features low noise of about 0.05% which is comparable to flight and an order of magnitude lower than conventional tunnels. This makes the BAM6QT unique for boundary-layer transition studies.

II. Boeing/AFOSR Mach-6 Quiet Tunnel

The BAM6QT is a Ludwieg tube, a long tube with a converging-diverging nozzle on the end. The flow then passes through the test section, diffuser, a second throat, and finally to the vacuum tank. Flow is initiated by bursting a double diaphragm that is located downstream of the diffuser. When the flow begins, an expansion wave travels upstream and then reflects between the end of the driver tube and the contraction. The pressure drops with each reflection, until it decreases to the point that the tunnel unstarts. Run times of three to five seconds are typical at present.

It is difficult to obtain quiet flow in a tunnel. The nozzle is polished to a mirror finish to avoid roughness-induced transition. The boundary layer is also sucked off through bleed slots at the throat, for quiet runs. This restarts a laminar boundary layer in the nozzle which is maintained through the test section. The air is filtered using a 1-micron particle filter to remove dust or other particles that may damage the nozzle. More details about the development of the BAM6QT and other quiet tunnels can be found in Reference 8.

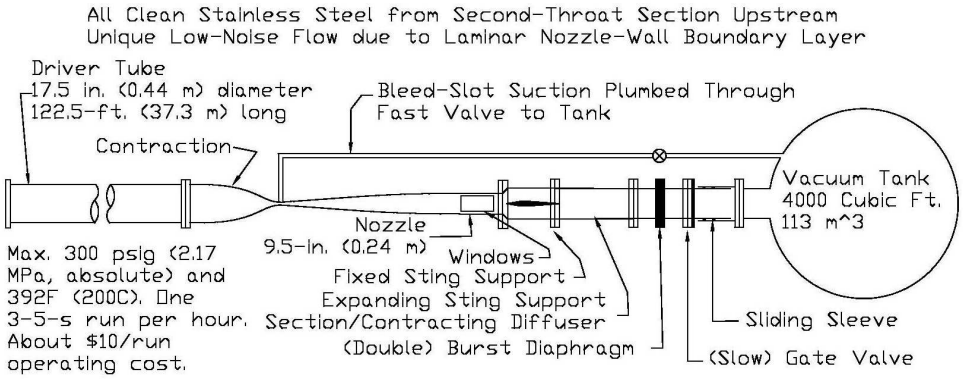

Figure 1: Boeing/AFOSR Mach-6 Quiet Tunnel

III. Temperature-Sensitive Paints

Temperature-sensitive paint (TSP)[9] is used to provide a qualitative measure of heat transfer and is useful for detecting increased surface heating from laminar-turbulent transition. When using TSP, a luminophore is excited by a light source and fluoresces. When the temperature of the luminophore is high, the intensity of the fluorescence decreases due to non-radiative energy-loss processes. From the ratio between a reference image at a known temperature and a second image, the surface temperature can be calculated. While the surface temperature distribution obtained from TSP measurements is quantitative, heat transfer calculations for the quiet tunnel are still unreliable. Current analysis techniques provide a limited ability to obtain quantitative data with thin insulator film on metal models or with nylon substrates. Possible sources of error include the

pressure dependence of the paint, the methods of reducing temperature to heat transfer, and unknowns in the substrate properties. Improved methods are needed and are being developed in order to obtain quantitative results and higher spatial and temporal resolution.[10]

Temperature-sensitive paints were used for wake visualization behind roughness elements on the HIFiRE forecone model and the nozzle wall. The TSP used was Ru(bpy) luminophore molecules in clear automotive paint. The paint is excited during a run with 464 nm light from a 4-in. diameter ISSI LM4 blue LED array. A calibration was conducted to relate the measured intensity ratio of the flow-off and flow-on photographs to the model surface temperature. A 12-bit Photometrics SensysB cooled CCD camera was used to capture all photographs. This camera can take 1 or 2 frames/sec, has 768×512 pixels, and each pixel is a $9\mu m$ square. The camera outputs a signal when the shutter is opened. That signal is recorded on an oscilloscope during the run and is used to calculate the Reynolds number and tunnel conditions for each image.

IV. Roughness-Induced Transition on the HIFiRE Forecone Model

The Hypersonic International Flight Research and Experimentation (HIFiRE) project is currently working to "develop and demonstrate fundamental hypersonic technologies deemed critical to the realization of next generation aerospace weapon systems."[11] This project involves several flight tests that will complement computations and ground experiments. The first flight is focused primarily on instrumentation. The performance of that instrumentation is being demonstrated through several sub-experiments studying boundary-layer transition, shock-boundary layer interaction, and optical measurements of mass capture in a duct. Kimmel[11] discusses the purpose and design methodology of the flight as well as the design of the boundary-layer transition sub-experiment. This sub-experiment will study boundary-layer transition behind a roughness element, as well as natural transition on the vehicle. In order to properly size the roughness element so that it will cause transition on the vehicle, wind tunnel tests of the HIFiRE vehicle near flight conditions were conducted in CUBRC[12] and also at NASA Langley Research Center[13] (NASA LaRC). Berger[13] discusses the trip sizing. The purpose of the BAM6QT tests was to show the effect of noise on those measurements. This was to help ensure that a roughness element designed using conventional wind tunnels was sized properly to ensure transition under quiet flight conditions. A parametric study of roughness height effects on transition was also conducted in the BAM6QT.

A. STABL computations for the HIFiRE Forecone Model

Preliminary STABL computations were completed in order to facilitate sizing a roughness element comparable to that in the NASA LaRC wind tunnel tests.[14] Johnson initially computed the mean flow over the model at 0° AoA at expected tunnel conditions. The displacement thickness at the roughness location was used to scale the roughness height from the NASA Langley tests. Once all tests were completed, the flow over the model at 0° and 6° AoA was recomputed using actual run conditions. These computations provided boundary-layer edge conditions and the roughness Reynolds numbers that were used to quantify the experimental results.

1. Mean Flow Solutions

For the axisymmetric mean flow solutions, 360×360 point structured grids were generated using STABL[15] with clustering both at the body surface and at the tip of the cone. The outer grid shape was specified to closely follow the shock. The three-dimensional mesh for the cone at angle of attack was generated using GridPro.[16] Clustering of points was applied near the body surface and near the tip of the cone, and grid tailoring was used to closely align the outer surface of the 3D grid to the shock shape. The 3D structured multi-block mesh consisted of hexahedral elements and contained approximately five million grid cells.

To ensure that the boundary layer solutions were well-resolved, grid point clustering in the body-normal direction was adjusted to obtain values of y^+ less than unity at the first solution point away from the wall. For the axisymmetric case, approximately half the total number of grid points were placed within the boundary layer. For the cone at angle of attack, approximately 40 grid points were used to resolve the boundary layer.

The laminar mean flow for the axisymmetric solution was generated using an optimized 2D/axisymmetric mean flow solver based on the implicit Data-Parallel Line Relaxation (DPLR) method.[17] The solver produces second-order accurate laminar flow solutions with low dissipation and shock capturing. The laminar

mean flow solutions for the 3D tests were generated using the unstructured 3D implicit solver US3D which implements the DPLR and full matrix point relaxation methods.[18] The gas used for the simulations was a single-species air model.

2. Mean Flow Integral and Roughness Calculations

Mean flow integral quantities such as the boundary-layer momentum thickness were calculated using the flow analysis features of STABL. The roughness Reynolds number was calculated as:

$$Re_k = \frac{\rho_k u_k k}{\mu_k}$$

where ρ_k, u_k and μ_k are the local density, velocity and viscosity all taken at the roughness height, k.

3. Stability Analysis

The PSE-Chem[15] code distributed with STABL was used for the LST and PSE boundary layer stability calculations. Chemistry and translational-vibrational energy exchange effects were turned off in the calculations to be consistent with the mean flow solver since, at the low free-stream enthalpies simulated here, chemistry plays a negligible role in the results.

For PSE calculations presented here, the N factor, which represents the log of the total amplitude growth of unstable boundary layer disturbances at particular frequencies, is defined as:

$$N(\omega, s) = \int_{s_0}^{s} \sigma ds$$

where ω is the frequency of a disturbance, s is the distance along the surface, s_0 is the location of the first critical point, and σ is the disturbance growth rate defined as:

$$\sigma = -Im(\alpha) + \frac{1}{2E}\frac{dE}{ds}$$

In this equation, α is the complex stream-wise wavenumber and E is the disturbance kinetic energy defined as:

$$E = \int_n \bar{\rho}\left(|u'|^2 + |v'|^2 + |w'|^2\right) dn$$

where $\bar{\rho}$ is the mean flow density, (u', v', w') are the complex fluctuating velocity components, and n is the direction normal to the body surface.

For LST calculations, the quasi-parallel flow assumption is made and the disturbance as a function of the body-normal coordinate only is solved for. This results in disturbance amplification rates, α_i, as a function of surface location and disturbance frequency where α_i is the imaginary part of the complex stream-wise wavenumber, and negative values indicate unstable disturbances. In the present stability analysis, only two-dimensional disturbances were considered.

B. HIFiRE Cone Model and Roughness Elements

The HIFiRE model is a seven-degree half-angle nylon cone with a 4-in. base diameter. This cone is a 36.9% model of the forecone of the HIFiRE vehicle with the exception of the nose radius. A stainless steel 0.047-in. radius nose was used. This radius was chosen to match the size of the full-vehicle models tested at NASA LaRC. The nylon portion stretches axially from 5.77 in. to 15.95 in. This section was painted with temperature-sensitive paint and used to visualize surface temperature. The nylon acts as an insulator and increases the temperature variations seen at the surface. Reference marks were applied for image alignment on the nylon frustrum. Reference marks are located on the windward ray and at ± 35 and 70 degrees. The marks are located 1 in. from the base of the model and spaced every 1.5 in. along the nylon portion of the cone.

A single roughness element was placed on the model for each run as shown in Figure 2b. Roughness elements were 0.05 by 0.05-in. squares, sized to match NASA LaRC's wind tunnel test trips. The trips were

made from plastic shims and glued to the model. Each trip was placed with a corner in line with the free stream and on the windward ray for all measurements at angle of attack. Johnson computed the mean flow over the model at estimated tunnel conditions. The displacement thickness at the roughness location was used to scale the roughness height from the NASA Langley tests. A trip height of 0.014 in. was found to match NASA LaRC's trip height of $3.2\delta^*$, though later computations at actual run conditions showed this trip height corresponded to $2.2\delta^*$, and a trip height of 0.021 in. corresponded to the desired height of $3.2\delta^*$. The trip was placed at an axial distance of 5.1 in. to equal the Re_{xk} for NASA LaRC at the BAM6QT maximum quiet pressure of 135 psia.

The 0.014-in. roughness height did not cause transition at zero angle of attack under quiet flow. In order to find an effective trip, higher roughness heights were then tested. Heights tested at zero angle of attack were 0.014, 0.018, 0.021, and 0.028 in, which corresponded to $2.2\delta^* - 4.3\delta^*$ per computations. At 6° angle of attack, the 0.014-in. high trip did cause transition when placed on the windward ray. Smaller trip heights of 0.004, 0.007, 0.011 in. were tested to find the limit of the trip effectiveness. A larger trip height of 0.028 in. was also tested. These heights corresponded to $1.1\delta^* - 7.7\delta^*$.

A typical model installation at zero angle of attack is shown in Figure 2. A number of variables were changed during tests. The model was tested at zero and six degrees angle of attack. The trip height was varied between 0.004 and 0.028 in. Most tests were run at 433 K initial stagnation temperature and at the maximum quiet pressure of the tunnel. The maximum initial stagnation pressure for quiet flow was 135 psia at the time of testing. This corresponded to a unit Reynolds number of 3.0×10^6/ft. A few runs were conducted at 5.6×10^6/ft under noisy flow (initial stagnation pressure of 255 psia) in order to match NASA LaRC test conditions.

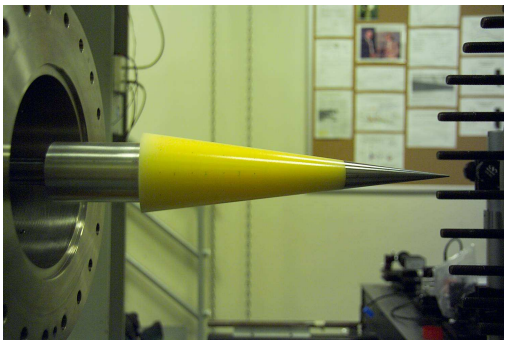

(a) Model setup in the BAM6QT

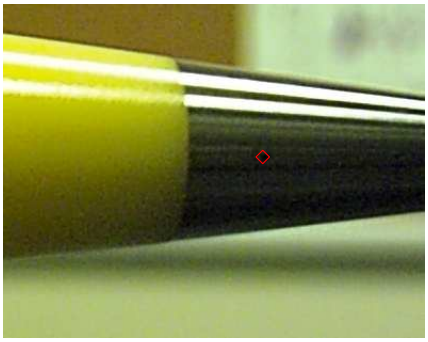

(b) Model view with red box showing location of roughness element

Figure 2: Model setup for testing in the BAM6QT, prior to installation of new sting support section in December 2007

Initial runs were conducted with the original smaller-diameter sting support and diffuser sections. These sections were replaced with larger-diameter sections prior to the second set of runs, in the hopes of starting larger models. A final data set was obtained with a 9-degree expansion ramp insert installed in the sting-support section. A discussion of these tunnel modifications can be found in Reference 19. The HIFiRE cone ran well for all tunnel configurations and no effect of changing tunnel configuration was observed in the temperature-sensitive paint results.

C. Data Presentation, Quality, and Uncertainty

The data presented below are surface temperature plots of the nylon portion of the cone. All measurements at angle of attack show the windward view unless otherwise specified. Noisy flow images are shown in the left column of each figure, and quiet flow images are on the right. Transition is inferred when the wake behind the trip starts to spread. This corresponded to a model surface temperature rise as shown in Figure 3. At the beginning of the temperature trace the flow is laminar. The temperature is low and has a small negative slope. This temperature decrease corresponds to the gradual thickening of the boundary layer along the model surface. The spikes in the trace occur at the model reference marks and should be ignored. A sharp rise in surface temperature is seen during transition, from 7.5 in. to approximately 10 in. in this case. The trace levels off again once turbulent flow is established on the model. The remainder of the temperature

trace has a small downward slope which is due to the growth of the now turbulent boundary layer. The centerline surface temperature rise showed transition onset more clearly than the surface temperature plots, and transition onset was consistently seen in the centerline temperature traces where the turbulent wedge was first visible in the surface temperature plots.

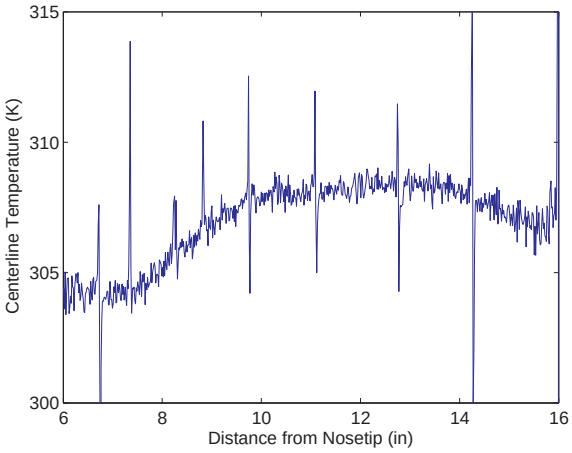

Figure 3: Typical centerline surface temperature distribution showing boundary layer transition

It should be noted that the BAM6QT has curved windows that conform to the interior of the wind tunnel. The windows act as lenses and distort images taken through them. The axial location of transition is not altered by the curved windows. The radial extent of the cone changes slightly, but not significantly. This radial distortion has not been corrected, as it does not interfere with comparing noisy and quiet effects or distort the transition location. It should also be noted that despite the use of a nylon model, the mean surface temperature of the model increases during the run, making it difficult to compare pictures taken at significantly different times during the run. There is also some variation in conditions when comparing data sets taken at similar times during the run. The transition location does not change noticeably for these variations. Many runs were repeated two times, and no noticeable change in the results, transition location, or transition footprint were found.

D. Results

1. Comparison of BAM6QT to NASA LaRC 20-in Mach 6 Air Tunnel

Several runs were conducted at conditions similar to NASA LaRC wind tunnel tests.[13] This was done to compare transition locations in the the NASA LaRC 20-in Mach-6 Tunnel to those found in the BAM6QT under noisy flow. Comparisons also help to validate data from the BAM6QT. The noise level of the NASA Mach-6 Tunnel (total pressure fluctuations) was reported as 2.8% in 2002. Mass flux and total temperature fluctuations at that time were reported as 2.4% and 1.4%, respectively.[20] Upgrades to the NASA Mach-6 Tunnel were completed since that time, and mass flux and total temperature fluctuations were remeasured and reported as 0.83% and 0.17%, respectively.[21] The total pressure fluctuation in the tunnel after these modifications was not found in the literature. The noise level of the BAM6QT (total pressure fluctuations) when run under noisy flow conditions is about 2-3% of the mean. How this compares to the total pressure fluctuations in the NASA LaRC 20-in. Mach-6 Tunnel is unknown.

A small subset of NASA LaRC's tests could be repeated. Only the 0.047-in. radius forecone model geometry was run in the BAM6QT. The Reynolds number of 5.6×10^6/ft as well as the location of the trip (2.7 in.) and the trip height (k=0.011 in.) were matched. TSP images in the BAM6QT were taken through a smaller porthole window that is rated for the higher pressures ($P_{0,i}$ = 255 psia) necessary to match the Reynolds number of the NASA LaRC runs. A comparison of the results from both tunnels under noisy flow at 0° AoA can be seen in Figure 4. The NASA LaRC images show quantitative heat transfer measurements using phosphor thermography. The red boxes on the NASA LaRC results show the portion of the HiFIRE forecone model imaged through the porthole windows in the BAM6QT.

Under noisy flow, the transition location and footprint is similar between the BAM6QT and the NASA

LaRC Mach-6 Tunnel. This smooth baseline transition location was also compared to computations performed by Alba et al.[22] for the 0.047-in. radius forecone in the NASA LaRC Mach-6 Tunnel. The transition location in the NASA tunnel is given at x/L = 0.65, though transition is non-uniform across the azimuth. When compared to computations, this gives a transition N-factor of 6.0. Transition in the BAM6QT was more uniform and occurred at x/L = 0.63 along the centerline. The transition N factor in the BAM6QT is 5.8 for this case. A N factor of 5.5 is a typical value for transition location in conventional noisy tunnels, which fits the experimental transition locations in the Purdue and NASA tunnels reasonably well. The relationship between noise and transition location remains a topic for future research.

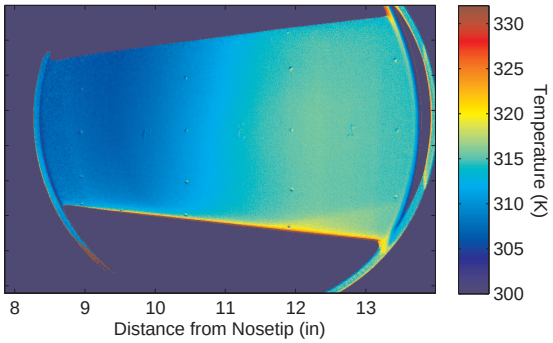

(a) BAM6QT, No trip, Re/ft=5.5 × 10^6

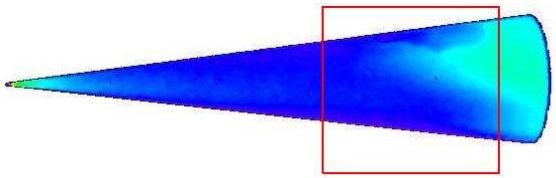

(b) NASA LaRC (HIFiRE Run 8), No Trip, Re/ft=5.6 × 10^6, from Ref. 23

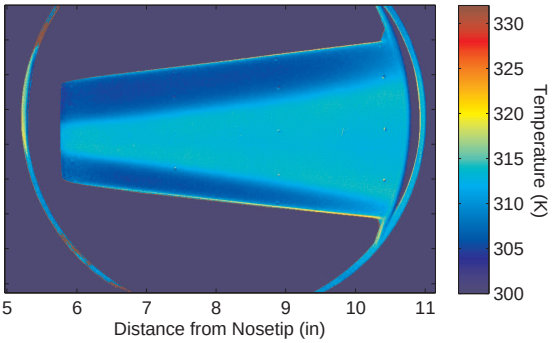

(c) BAM6QT, k = 0.011 in, Re/ft=5.5 × 10^6

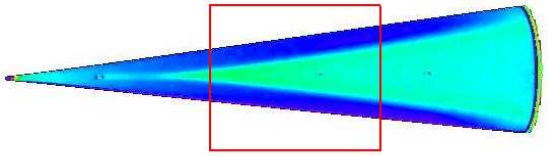

(d) NASA LaRC (HIFiRE Run 62), k = 0.0115 in, Re/ft=5.6 × 10^6, from Ref. 23

Figure 4: Comparison of transition at 0° AoA in NASA LaRC 20-in Mach-6 Air Tunnel to BAM6QT under noisy flow

E. Baseline Model Transition under Noisy and Quiet Flow

The HIFiRE forecone model was tested with no trip to obtain a baseline comparison between quiet and noisy flow. Figure 5 shows the cone at zero angle of attack under both noisy and quiet flow. Transition is apparent in the noisy flow case. The transition front is approximately 10% asymmetric, possible due to a small angle of attack on the model, flow nonuniformity, or paint imperfections. Under quiet flow, the boundary layer remains laminar to the end of the model. A drastic difference between noisy and quiet flow is also seen at angle of attack. Figure 6 shows the model at six degrees angle of attack with no trip. Both side and windward views are shown. Under noisy flow, transition begins away from the windward side. Figure 6c shows that transition then appears to propagate towards the windward ray. Under quiet flow, laminar flow is maintained to the end of the cone. Crossflow vortices are visible under quiet flow, and may be the cause for natural transition under noisy flow at angle of attack. These have been seen under noisy flow by Swanson[24] but are not apparent in this case. These results are typical of blunt cones studied previously in the BAM6QT.

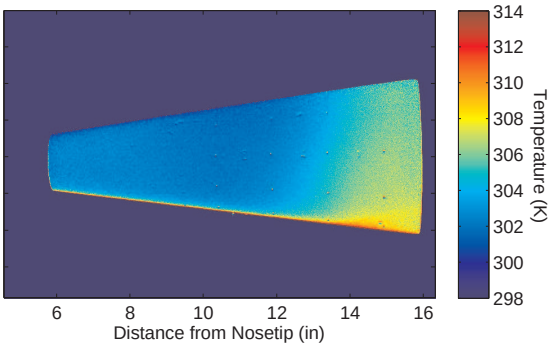

(a) P_o=139 psia, T_o=428 K, t=0.97s, Re/ft=3.2 $\times$ 10^6, Noisy Flow

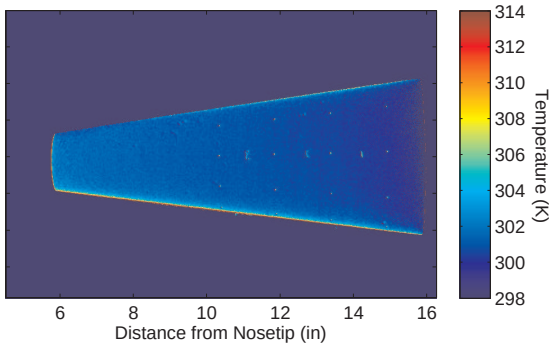

(b) P_o=129 psia, T_o=427 K, t=0.75s,Re/ft=3.0 $\times$ 10^6, Quiet Flow

Figure 5: Natural transition under noisy and quiet flow at 0° AoA

1. *Effect of Trip Height*

A parametric study of trip height was conducted at both zero and six degrees angle of attack. Figure 7 shows the model under noisy and quiet flow at zero angle of attack for increasing trip heights. Flow conditions for each image as well as the measured transition locations at 0° AoA are found in Table 1. In all cases, two straight streaks can be seen in the wake of the roughness element. Several inches downstream of the trip, the wake spreads and a turbulent wedge appears. Transition is inferred at this location, when a rise is also seen in the centerline surface temperature. Figure 8 plots the roughness Reynolds number for each trip height against the transition onset location under both noisy and quiet flow. The smallest trip height corresponds to the smallest roughness Reynolds number. A noticeable difference between the noisy and quiet flow conditions can be seen. The same trip heights that caused transition on the model under noisy flow did not necessarily cause transition on the model in quiet flow. When transition did occur, it was delayed. The ratio of transition Reynolds numbers under noisy and quiet flow at 0° AoA can be seen in Table 2. An increase of up to 6.4 times the noisy transition Reynolds number when referenced to the trip location was observed under quiet flow. When referenced to the nose, the transition Reynolds number increased by factors of up to 2.2.

Under noisy flow, it is interesting to note that the transition location behind the roughness element does not noticeably change with increasing trip height, beyond a point. The smallest roughness height of 0.014 in. is not fully effective at 0° AoA. However, the 0.018-in. trip as well as the 0.021 and 0.028-in. trips cause transition at approximately the same location on the model. This indicates that a 0.018-in. trip may be fully effective under noisy flow. Under quiet flow, the 0.014-in. high trip generated a pair of vortices, but the flow remains laminar to the end of the cone. The 0.018-in. high trip also generated two streaks in its wake, and transition begins just before the end of the model. The 0.021 and 0.028-in. high trips both caused transition downstream of the trip, but the transition location does not change significantly between these two trip heights (Figure 8). This may indicate that the effective transition height for quiet flow conditions has nearly been reached. It would be interesting to test higher trips to see if the transition location can be moved further forward under both noisy and quiet flow conditions and to confirm when an effective trip height has been reached.

For a less-than-effective trip under quiet flow, there was a significant difference between quiet and noisy flow transition locations. For example, a trip height of 0.018 in. (less-than-effective under quiet flow) delayed transition by 6.4 times when referenced to the trip location and 2.2 times when referenced to the nose. Berry and Horvath[25] recently hypothesized that tunnel noise would "have an effect on the transition process only when the trips are less than fully effective." However, a delay in the transition location was still seen with effective trips under quiet flow when compared to noisy flow results. For an effective trip under both quiet and noisy flow, the ratio of the quiet to noisy transition Reynolds number was 2.1 when referenced to the trip location and 1.3 when referenced to the nose. The difference in transition location between quiet and noisy flow conditions is significantly reduced when effective trips are used, but quiet flow still delays the transition location for an effective trip. A similar result was seen for experiments at angle of attack.

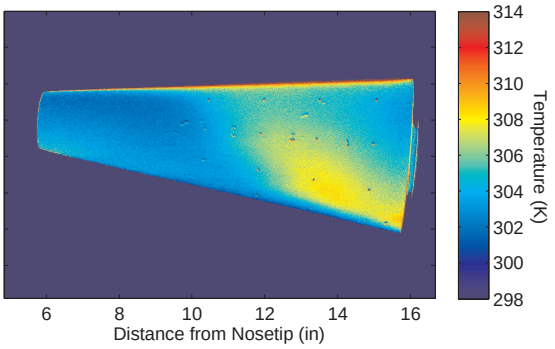

(a) P_o=129 psia, T_o=426 K, t=0.80s, Re/ft=3.0 $\times 10^6$, Noisy Flow, Side View

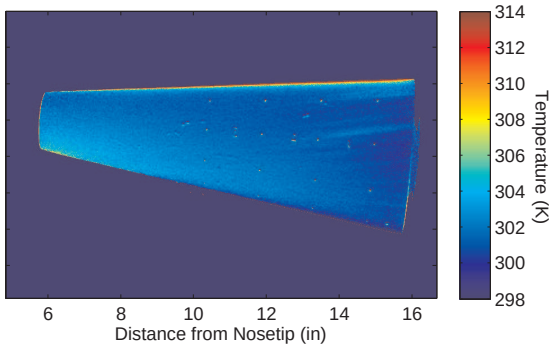

(b) P_o=131 psia, T_o=429 K, t=0.77s, Re/ft=3.0 $\times 10^6$, Quiet Flow, Side View

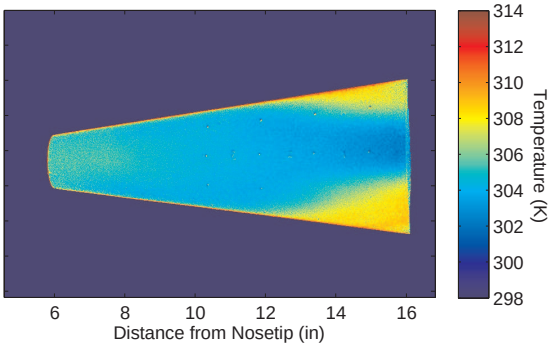

(c) P_o=132 psia, T_o=429 K, t=0.85s, Re/ft=3.0 $\times 10^6$, Noisy Flow, Windward View

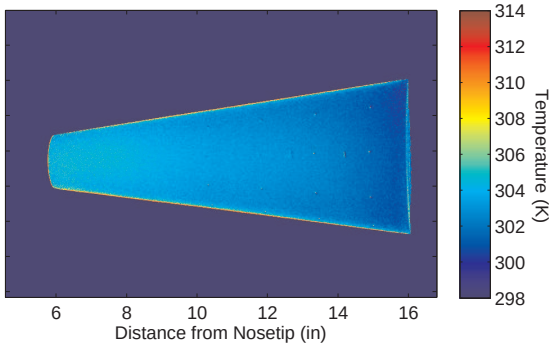

(d) P_o=126 psia, T_o=425 K, t=0.99s, Re/ft=2.9 $\times 10^6$, Quiet Flow, Windward View

Figure 6: Natural transition under noisy and quiet flow at 6° AoA

noisy/quiet	k (in.)	P_0 (psia)	T_0 (K)	t (s)	Re/ft $\times 10^{-6}$	x_{tr} (in)
noisy	0.014	129	427	1.1	2.9	7.3
noisy	0.018	129	426	1.2	3.0	6.5
noisy	0.021	128	426	1.3	2.9	6.8
noisy	0.028	131	427	1.0	3.0	6.7
quiet	0.014	128	425	0.89	2.9	n/a
quiet	0.018	125	423	1.2	2.9	14
quiet	0.021	127	425	1.0	2.9	8.5
quiet	0.028	126	424	1.1	2.9	8.5

Table 1: Image conditions and transition location for various trip heights at 0° AoA. Trip located at 5.1 in.

k (in.)	k/δ^*	Re_k	Delay Factor Referenced from Trip	Delay Factor Referenced from Nose
0	0	0	> 2.2	> 1.6
0.014	2.2	120	> 5.0	> 2.2
0.018	2.8	230	6.4	2.2
0.021	3.2	380	2.0	1.3
0.028	4.3	1500	2.1	1.3

Table 2: Quiet to noisy ratio of transition Reynolds number referenced to both the trip location and nose at 0° AoA

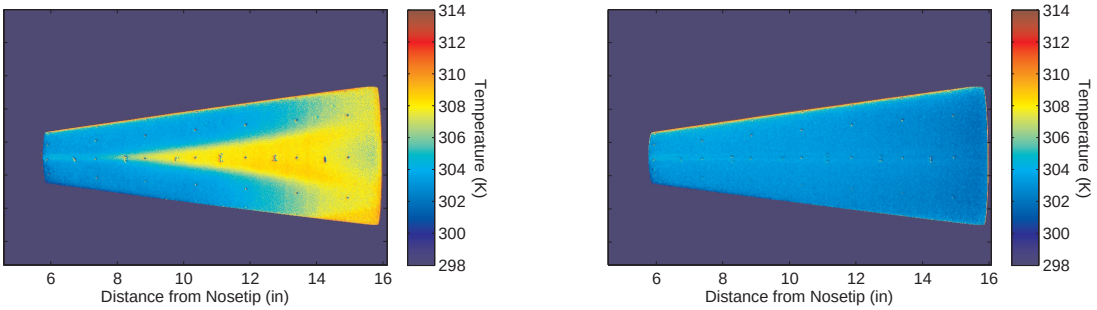

(a) k=0.014 in.

(b) k=0.014 in.

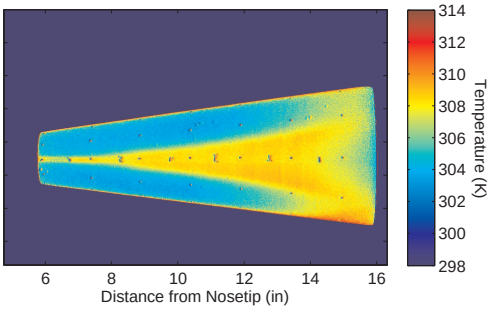

(c) k=0.018 in.

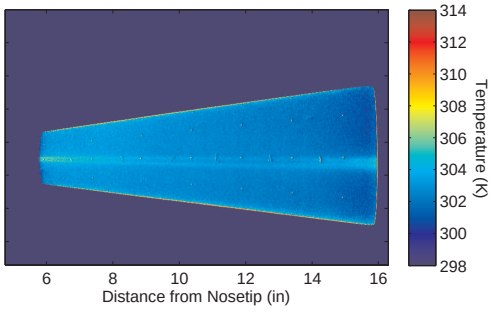

(d) k=0.018 in.

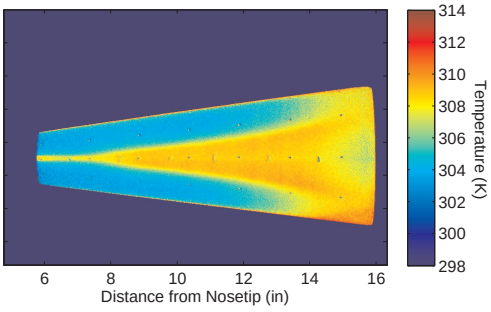

(e) k=0.021 in.

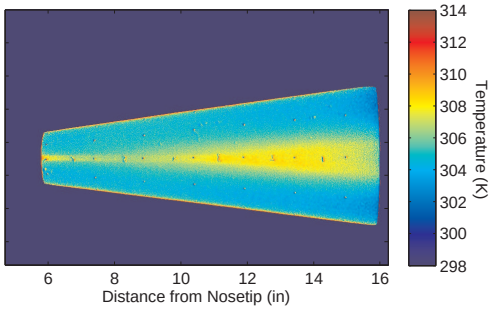

(f) k=0.021 in.

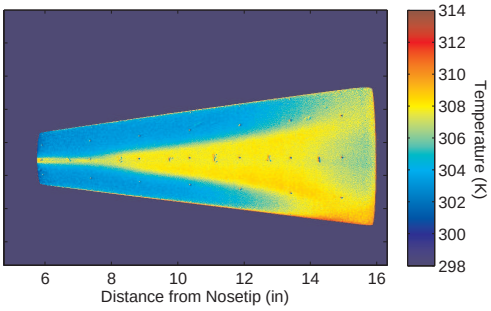

(g) k=0.028 in.

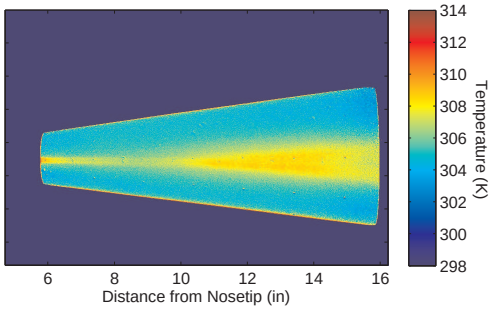

(h) k=0.028 in.

Figure 7: Effect of trip height under noisy and quiet flow at 0° AoA. Noisy flow is shown in left column and quiet flow in right column.

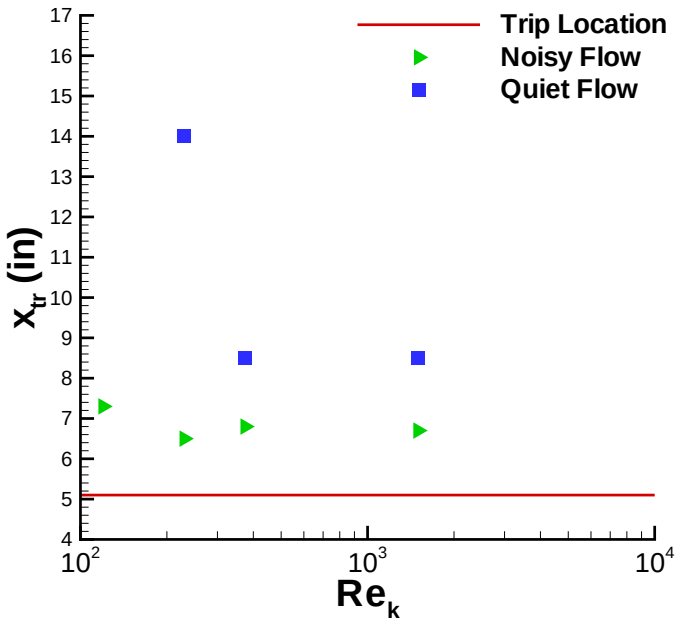

Figure 8: Effect of trip Reynolds number on transition location at 0° AoA

2. Angle of Attack Effects

The trip height was again varied on the HIFiRE model at 6 degrees angle of attack. The windward boundary layer is thinner at angle of attack, which makes smaller trip heights more effective. Trip heights ranging from 0.004 in. to 0.028 in. were tested, which corresponds to trip heights of 1.1 to 7.7 times the boundary layer displacement thickness at the trip location. Figure 9 shows the resulting surface temperature plots for increasing trip heights under noisy flow (left column) and quiet flow (right column). Flow conditions for each image as well as the measured transition locations are found in Table 3. Once again, quiet flow has a marked effect on roughness-induced transition. Transition under quiet flow is delayed as shown in Figure 10. This delay translates into an increase of the transition Reynolds number (Table 4).

Under noisy flow, the 0.004-in. trip generates two vortices, and transition occurs well downstream of the trip. This trip is somewhat less than effective for noisy flow. The 0.007 and 0.011-in. trips both generate two vortices. Transition occurs approximately 1.3 in. downstream of the trip. The transition location seems to remain constant between these two trip heights, indicating that a 0.007-in. trip is effective under noisy flow. At the higher trip heights of 0.014 and 0.028 in, the transition footprint looks different, though transition still occurs 1.3 in. behind the trip along the model centerline. This can be seen in the centerline temperature traces in Figure 11. The temperature behind the roughness element is very high, possibly because of the strong vortices generated by the trip. Transition onset is taken where the centerline temperature begins to rise. The transition front is much wider and is actually composed of three merging turbulent wedges. This pattern is seen more clearly under quiet flow. Streaks behind the roughness element are seen well into the turbulent regions, suggesting that the vortices generated by the trip continue even under turbulent flow.

The behavior is similar under quiet flow, though delayed. In the case of the shortest trip, neither the presence of vortices nor transition is seen on the cone. For the 0.007-in. trip, transition is delayed by a factor of 4.8 when referenced to the trip location and 1.8 when referenced to the nose. Transition behind the 0.011-in. trip is delayed under quiet flow by 3.5 when referenced to the trip location and 1.5 when referenced to the nose. It is interesting to note that the two vortices generated by the trip curve away from each other in these cases. This spanwise spreading of the streamwise vortices could indicate outward-directed crossflow. Transition is again delayed at trip heights of 0.014 and 0.028 in. The transition onset location continues to move forward with increasing trip height, making it unclear whether the 0.028-in. trip is fully effective under quiet flow (Figure 10). Also, a marked change in the temperature surface plots is again seen at higher

trip heights of 0.014 and 0.028 in. Instead of two vortices, six streaks are evident behind the roughness element. Each pair of streaks leads to the formation of a turbulent wedge and transition. This was seen under noisy flow, but is much clearer under quiet flow (particularly with the 0.028-in. trip). Transition behind the roughness elements is asymmetric for both these conditions. The reason for this asymmetry is unknown. Streaks are again evident well into the turbulent region in the case of the 0.028-in. trip. Higher heating around the multiple streaks suggests that strong vortices are generated.

noisy/quiet	k (in.)	P_0 (psia)	T_0 (K)	t (s)	Re/ft $\times 10^{-6}$	x_{tr} (in)
noisy	0.004	131	428	0.89	3.0	8.5
noisy	0.007	129	427	1.1	3.0	6.4
noisy	0.011	130	429	0.79	3.0	6.5
noisy	0.014	136	427	1.0	3.1	6.4
noisy	0.028	130	427	1.0	3.0	6.4
quiet	0.004	128	426	0.89	3.0	n/a
quiet	0.007	120	418	1.8	3.0	11.3
quiet	0.011	130	426	0.78	3.0	10
quiet	0.014	130	425	0.91	3.0	8
quiet	0.028	129	416	0.79	3.0	7

Table 3: Image conditions and transition location for various trip heights at 6° AoA. Trip located at 5.1 in.

k (in.)	k/δ^*	Re_k	Delay Factor Referenced from Trip	Delay Factor Referenced from Nose
0	0	0	unknown	unknown
0.004	1.1	30	> 3.2	> 1.9
0.007	1.9	100	4.8	1.8
0.011	3	340	3.5	1.5
0.014	3.8	860	2.2	1.3
0.028	7.7	6900	1.5	1.1

Table 4: Quiet to noisy ratio of transition Reynolds number referenced to the trip location and nose at 6° AoA

Multiple vortices behind a roughness element have been seen before. Whitehead[26] saw multiple vortices in oil flow experiments over various roughness geometries (Figure 12). He noted several "counter rotating vortex filaments which initiate ahead of the element and are forced downstream around the element." His oil flow images shows the interaction of the separation region in front of the element and the bow shock from the trip itself. A simplified flow-field schematic is shown in Figure 13. On the HIFiRE model, multiple vortices may have been generated by the smaller trip heights, but they may be too weak to be seen in the surface temperature plots. On the other hand, the flow-field around the roughness element may be different with smaller roughness heights, leading to the formation of only two vortices in the wake of the roughness element.

3. Comparison with other Roughness-Induced Transition Data on Cones

The HIFiRE results for effective trips under noisy and quiet flow at zero and six degrees AoA are plotted in Figure 14 against a summary of sharp cone data from Reference 1. Transition occurs much sooner behind the transition element when compared to sharp cone data. It would be useful to compare this HIFiRE data against existing data on blunt cones if it can be found.

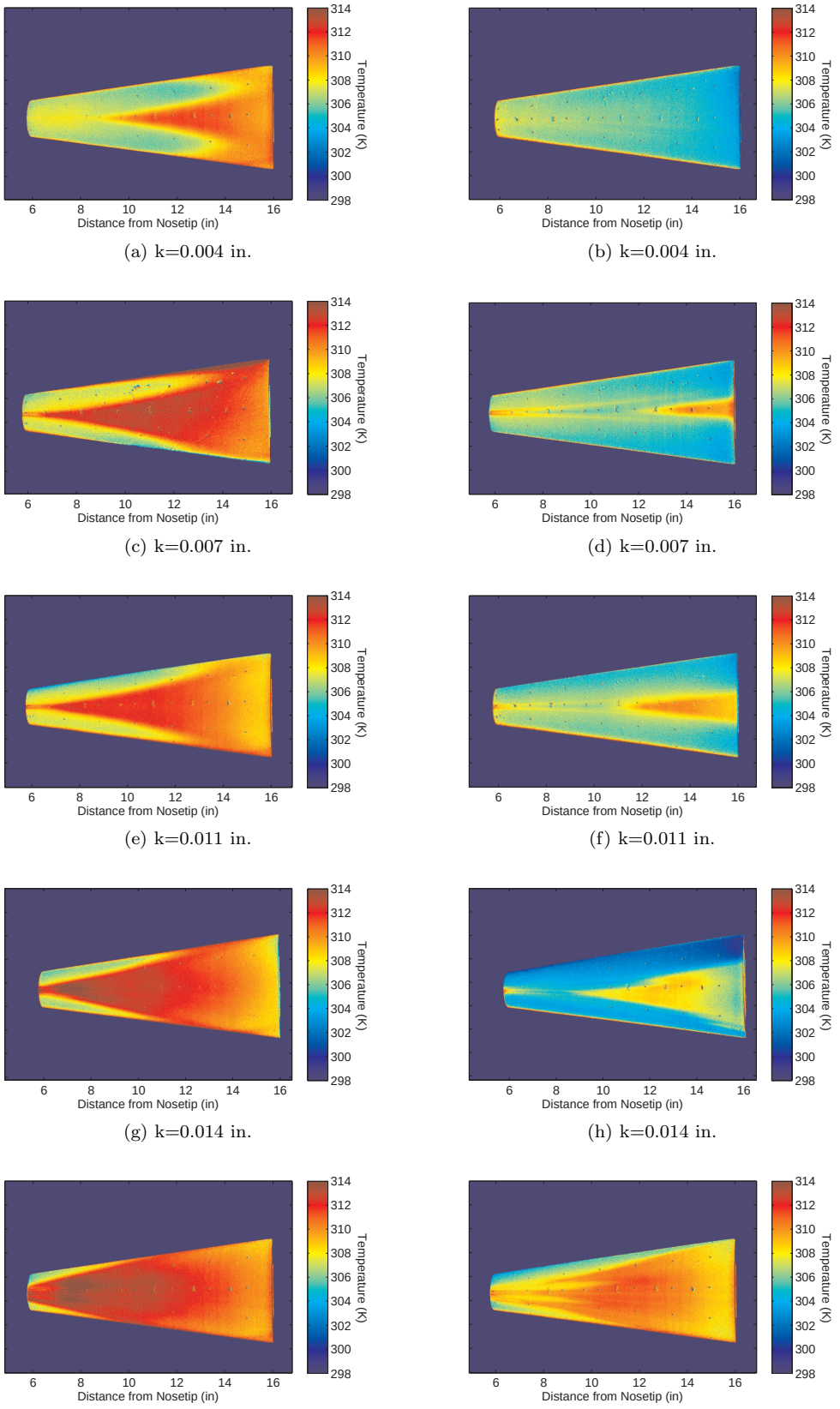

(a) k=0.004 in.

(b) k=0.004 in.

(c) k=0.007 in.

(d) k=0.007 in.

(e) k=0.011 in.

(f) k=0.011 in.

(g) k=0.014 in.

(h) k=0.014 in.

(i) k=0.028 in.

(j) k=0.028 in.

Figure 9: Effect of trip height under noisy and quiet flow at 6° AoA. Noisy flow is shown in left column and quiet flow in right column.

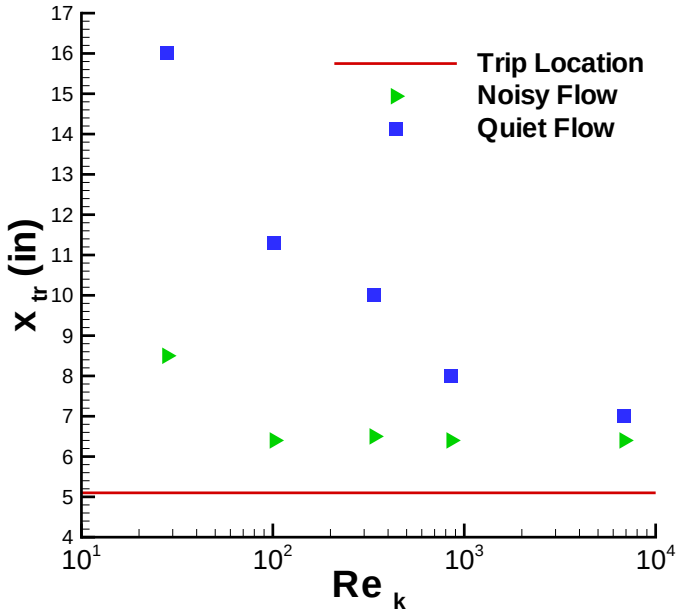

Figure 10: Effect of trip Reynolds number on transition location at 6° AoA

4. Summary and Future Work

A parametric study of isolated roughness height on the scaled forecone of the HIFiRE Flight 1 payload was conducted in the BAM6QT. Tunnel noise was shown to have a significant effect on transition location. The effective height found in a conventional tunnel may be insufficient to ensure transition in flight. Transition was delayed under quiet flow by factors of up to 6.4 (for a less-than-effective trip) when referenced to the trip location and by 2.2 when referenced to the nose. Effective trip heights under both noisy and quiet flow still caused later transition under quiet flow, though the delay in transition is reduced when compared to a less-than-effective quiet flow trip. Future work should include TSP measurements near the roughness element itself. These results could be compared to Whitehead's oil flow experiments, and the flow field differences around the roughness elements when two vortices or six vortices are seen in the TSP results could be explored. Also, traditional schlieren or background oriented schlieren imaging around the roughness element (although not possible at present in BAM6QT) would be useful to visualize the bow shock generated by the trip. Finally, exploring higher roughness heights, particularly at 0° AoA, would help clarify if a higher roughness element will move transition forward and generate six vortices in its wake as was seen with the model at angle of attack.

V. Effect of an Isolated Roughness on the Nozzle Wall Boundary Layer

A. Background

The effect of an isolated roughness on transition is being studied in an effort to develop a semi-empirical physics-based method for predicting transition. The BAM6QT features a unique laminar boundary layer. At lower Reynolds numbers, it is up to 3/4 in. thick on the nozzle wall. This boundary layer is thicker than that found on models and it is easier to make precise measurements using methods such as hot-wire anemometry. Because of the thick laminar boundary layer, measurements of the growth of instabilities should be more feasible. These measurements will be useful in understanding the mechanisms that lead to transition.

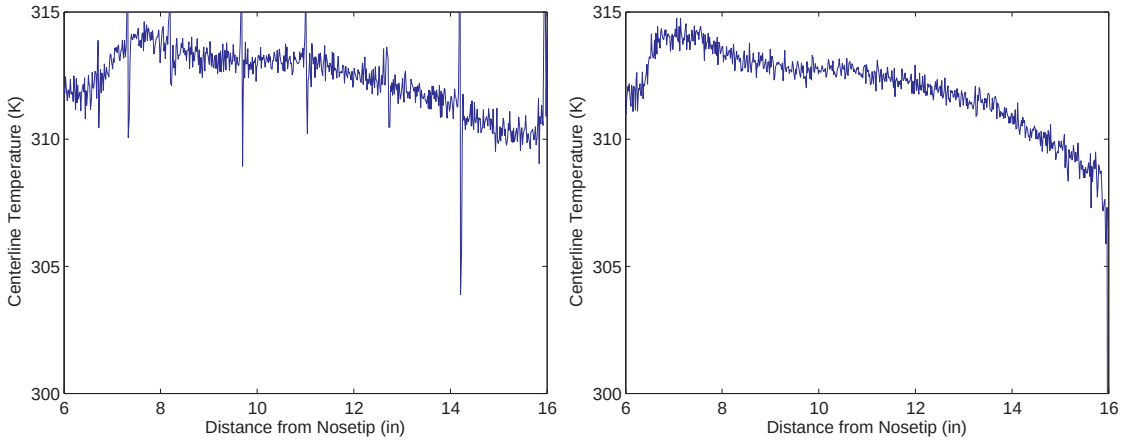

(a) k = 0.014 in. (b) k = 0.028 in.

Figure 11: Centerline temperature trace under noisy flow at 6° AoA

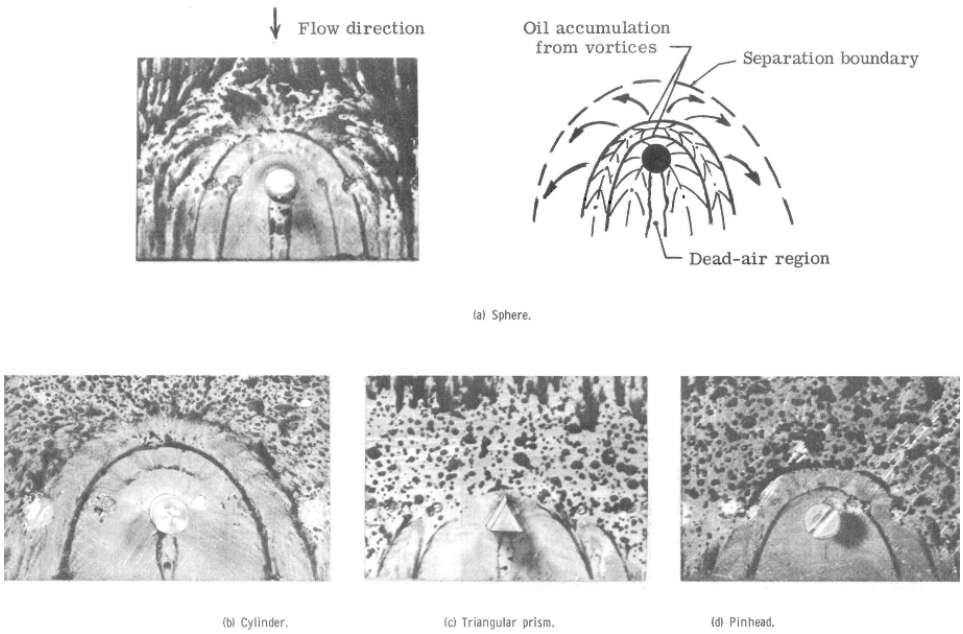

Figure 12: Oil flow on various trip geometries in hypersonic flow, from Ref. 26

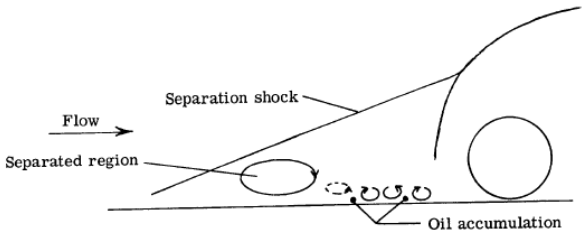

Figure 13: Simplified flow-field schematic for spherical element, from Ref. 26

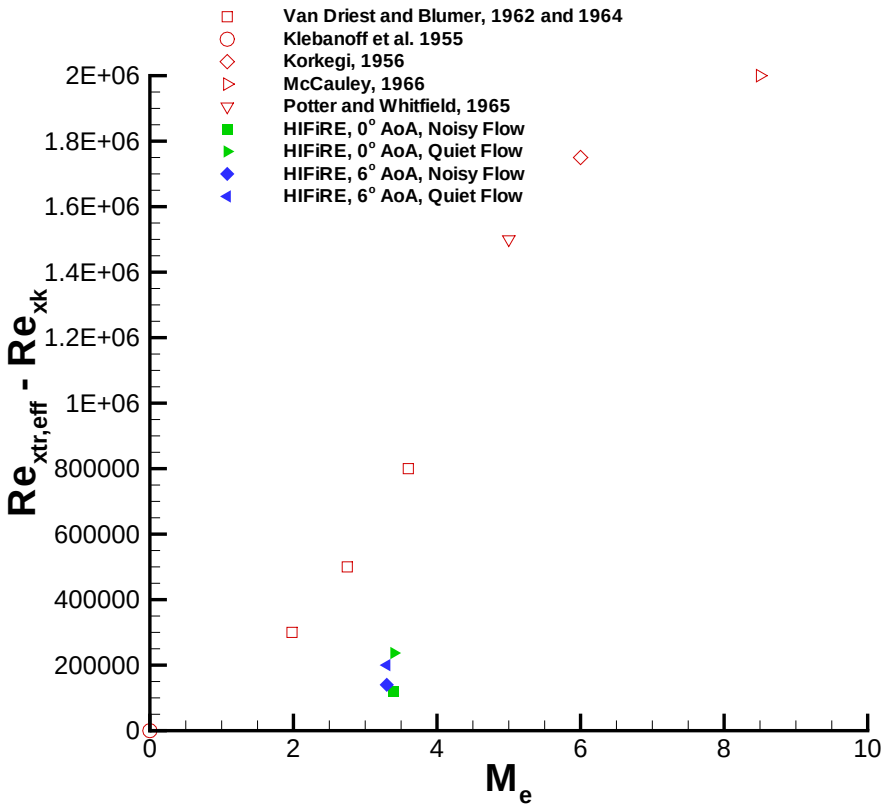

Figure 14: Variation with Mach number of Reynolds number based on trip to transition on cones

B. Experimental Setup for Initial Wake Measurements

Temperature-sensitive paint was used to visualize the temperatures in the wake behind an isolated roughness element. The TSP measurements were intended to identify preliminary flow features within the wake at various initial stagnation pressures. A diagram of the location of the roughness element and the region examined using TSP appears in Figure 15.

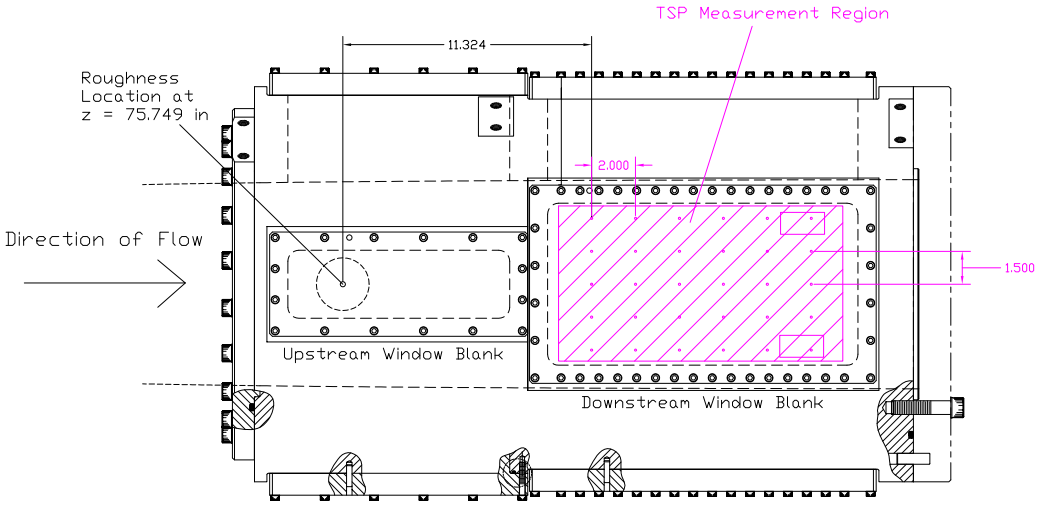

Figure 15: Diagram of roughness location and TSP measurement region in the BAM6QT test section. Dimensions in inches.

1. *Roughness Element*

A 0.235-in.-diameter micrometer head (Starrett model 263L–38TN) was used as a roughness element. The height of the roughness element can be changed from $k = 0.000$ in. to $k = 0.957$ in. and is accurate to ± 0.002 in. The roughness element was located in the test section of the BAM6QT at tunnel coordinate z = 75.749 in., mounted in a specially designed circular insert in the upstream window blank. Figures 16 and 17 show the roughness insert mounted in the window blank. Three locations in the circular insert allow the spanwise position of the roughness element to be changed, so that measurements can be taken off the center of the wake. Roughness height was adjusted prior to each test using the micrometer.

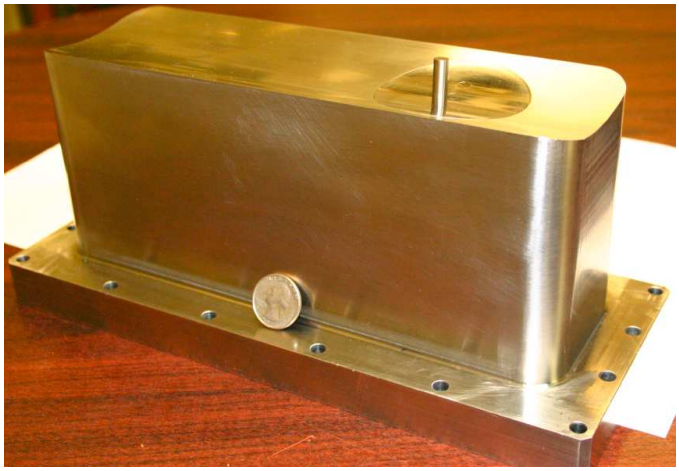

Figure 16: Roughness element with circular insert installed in forward window blank.

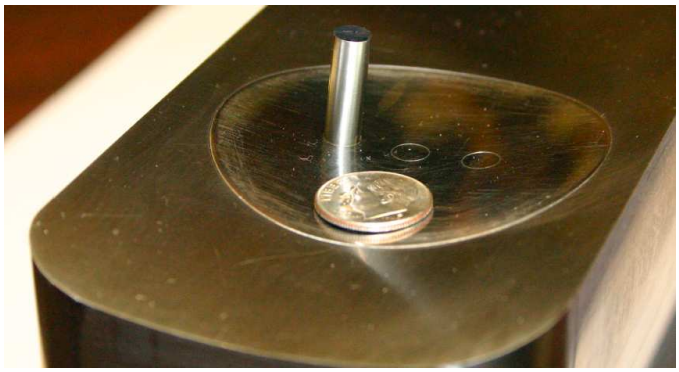

Figure 17: Roughness element. Micrometer head with 0.235 in. diameter. Three spanwise positions can be measured by moving the roughness element.

2. Temperature-Sensitive Paint (TSP)

TSP was used in this experiment to examine the flow features in the wake behind the roughness element. The inside of the large window blank downstream of the roughness was covered with a 0.0045-in.-thick adhesive-backed PVC insulator. The insulator layer was applied carefully to limit the occurrence of air bubbles, though the variable radius of curvature of the window blank made this difficult. Some air bubbles developed during testing and are visible in the TSP photos.

The insulator was spray-painted with Ru(Bpy) dissolved in ethanol, mixed with Nason 496-00 clear automotive paint and activator. Registration marks were applied at a 2-in. axial spacing and 1.5-in. vertical spacing, beginning at z = 87.1 in. (about 11.3 in. downstream of the roughness element). These marks were used for image alignment and flow feature location.

C. Preliminary TSP Results

Temperature-sensitive paint images of the wake of the isolated roughness element were obtained to provide an understanding of the flow behind the roughness element. In the images, flow is from left to right. The images were taken at an initial tunnel stagnation pressure of 120 psia and an initial stagnation temperature of 473 K with varying roughness height, k. Temperatures were calculated from a TSP calibration of the ratio of flow-on intensity to flow-off intensity. The boundary layer thickness δ was calculated from computations at 130 psia stagnation pressure, and scaled to the actual stagnation pressure using the square root of the Reynolds number. In the computations, δ was assumed to be the height above the wall at which the velocity is 99.95% of its freestream value.

Air bubbles from underneath the PVC insulator appear in the images as dark blue marks. The bubble heights of approximately 0.01 in. were relatively small compared to the boundary layer thickness and thus should not have affected the flow. Two layers and three layers of plastic insulator were applied on rectangular patches at the downstream end of the window blank, off the centerline, as part of a separate TSP sensitivity experiment.

1. Laminar vs. Turbulent Boundary Layer Images

The effect of a laminar and turbulent nozzle wall boundary layer on the wake of the roughness element is shown in Figure 18. Two images are shown with a roughness height of 0.10 in. ($\frac{k}{\delta} \approx 0.32$) at similar stagnation pressure. In the first image, the nozzle wall boundary layer is turbulent, corresponding to noisy flow. In the second image, the nozzle wall boundary layer is laminar, corresponding to quiet flow.

The flow field behind the roughness element is quite different depending on the condition of the nozzle wall boundary layer. During noisy flow, the incoming boundary layer is turbulent and the wake region is much wider than in quiet flow. In addition, the heating is higher overall within the wake. When the incoming boundary layer is laminar the wake of the roughness is visible as two thin streaks which spread as they progress downstream. Experiments in a laminar nozzle wall boundary layer cannot be carried out except under quiet conditions, at present. Under noisy conditions, the nozzle wall boundary layer is always

turbulent. Comparisons of the effect of tunnel noise on a laminar boundary layer, such as in Figure 5, are not feasible, as the BAM6QT can only operate with a laminar boundary layer on the nozzle wall during quiet conditions.

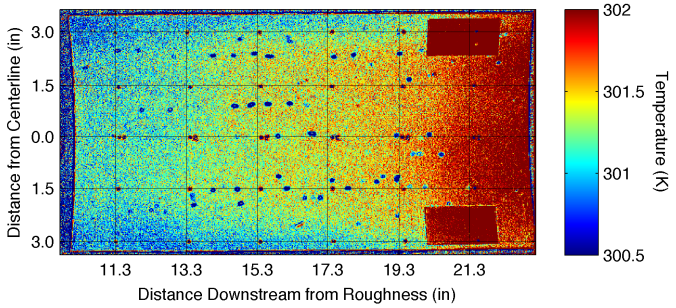

(a) Noisy flow, $P_0 = 109.9$ psia, Re/ft $= 2.6 \times 10^6$.

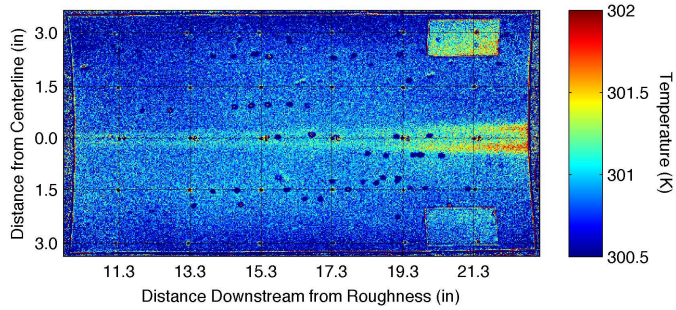

(b) Quiet flow, $P_0 = 107.9$ psia, Re/ft $= 2.4 \times 10^6$.

Figure 18: Roughness wake temperatures when $P_{0,i} = 120$ psia, $k = 0.10$ in, and $\frac{k}{\delta} \approx 0.32$. Noisy vs. quiet flow at $t = 1.5$ s.

2. Roughness Height Effects on a Laminar Boundary Layer

The effect of increasing roughness height on wake temperatures in a laminar boundary layer is shown in Figures 19 through 22. Each figure shows four TSP images from the same run in chronological order. As the run progresses, the tunnel stagnation pressure decreases, the unit Reynolds number decreases, and the boundary layer thickness increases.

Figure 19 shows images with a roughness height of 0.18 in., corresponding to $\frac{k}{\delta} \approx 0.58 - 0.55$. The run was quiet with bleed suction on, and all four images were taken during the quiet portion of a single run. The images show a long, thin streak of a higher temperature wake region behind the roughness element. Farther downstream, spreading of the higher temperature region occurs. As the run progresses, the temperature of the wake region decreases slightly. The decrease in temperature could be due to decreased heat transfer from the thickening boundary layer as the run progresses.

Figure 20 shows images from a quiet run when k is increased from 0.18 in. to 0.26 in. In these images, $\frac{k}{\delta}$ decreases from 0.86 to 0.82. The high temperature wake region becomes much more pronounced after the increase in roughness height. The wake is still centered behind the roughness element but is much wider. Four-to-six hot streaks are visible during the run. As the run progresses, the temperature in the wake changes. The first photo shows many hot streaks and a larger spreading angle. Eventually, the number of hot streaks decreases to four and the outside streaks develop farther downstream than the inside streaks.

Figure 21 shows images from a quiet run where $k = 0.40$ in. and $\frac{k}{\delta} \approx 1.27 - 1.22$. The roughness height now exceeds the boundary layer thickness. The photos show that the wake region is now wider and seems to remain wide throughout the run, though temperatures decrease during the run. Hot streaks are still visible at this roughness height, with four to six visible in the first photo. During this run, the wake begins to encroach on the regions with double and triple layers of insulator. The thicker insulator layer decreases the heat transfer to the nozzle wall, resulting in higher temperatures.

Figure 22 shows the case of a roughness height of 0.76 in. and $\frac{k}{\delta} \approx 2.42 - 2.32$, which is well outside of the boundary layer. Again, this run was quiet with a laminar boundary layer on the nozzle wall. A wide wake region is visible in the images, with thick hot streaks that decrease in temperature as the run progresses.

D. Summary and Planned Future Work

These images provide preliminary results from experiments on the nozzle wall at one initial tunnel stagnation pressure. The images offer a glimpse of the flow features found in the wake of the isolated roughness. As roughness height is increased in a laminar boundary layer, the wake region widens and several hot streaks become visible. The hot streaks may be developing vortices or other disturbances in the flow. Though temperature-sensitive paint images are useful in identifying flow features such as these hot streaks, the flow features need to be studied using other instrumentation such as hot films or hot wires. Measurements of the growth of instabilities within the nozzle wall boundary layer should be performed with and without the roughness element at varying streamwise locations.

Acknowledgments

This work could not have been completed without the help of many individuals. The Ludwieg Tube Group (Matt Borg, Michael Hannon, Tom Juliano, and Erick Swanson) and Justin Rubal provided advice and suggestions throughout the project. Thanks is also extended to Roger Kimmel for help in planning the HIFiRE BAM6QT experiments. This work was funded in part by the National Defense Science and Engineering Graduate Fellowship, Sandia National Laboratories, AFOSR, and the NASA Fundamentals program.

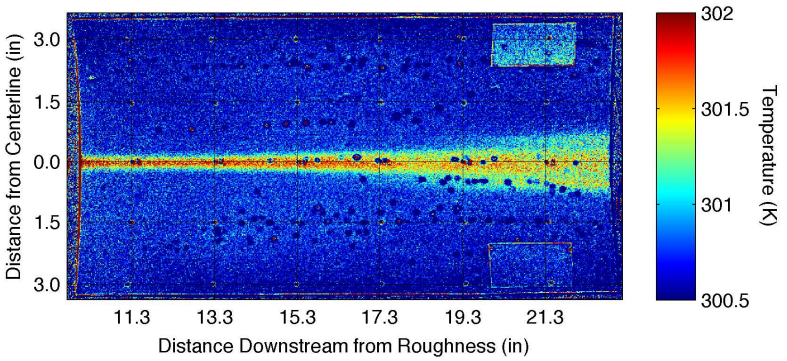

(a) $t = 1.52$ s, $P_0 = 108.3$ psia, $\frac{k}{\delta} \approx 0.58$, Re/ft $= 2.45 \times 10^6$.

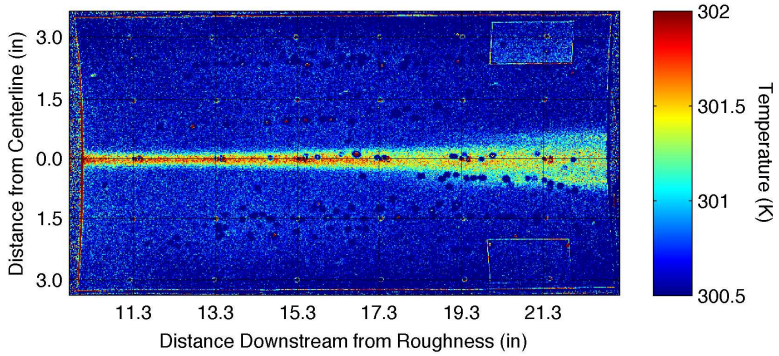

(b) $t = 1.98$ s, $P_0 = 105.6$ psia, $\frac{k}{\delta} \approx 0.57$, Re/ft $= 2.39 \times 10^6$.

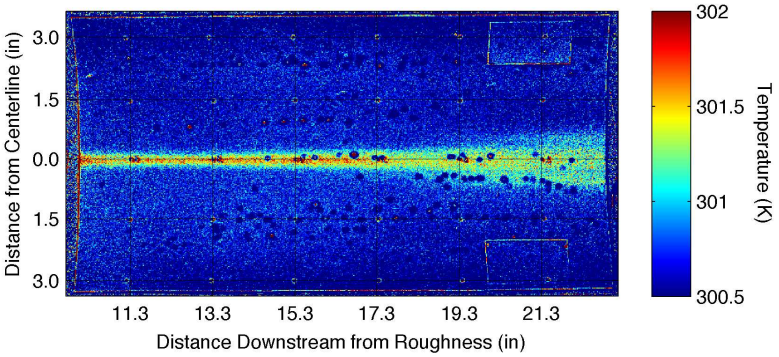

(c) $t = 2.44$ s, $P_0 = 101.7$ psia, $\frac{k}{\delta} \approx 0.56$, Re/ft $= 2.30 \times 10^6$.

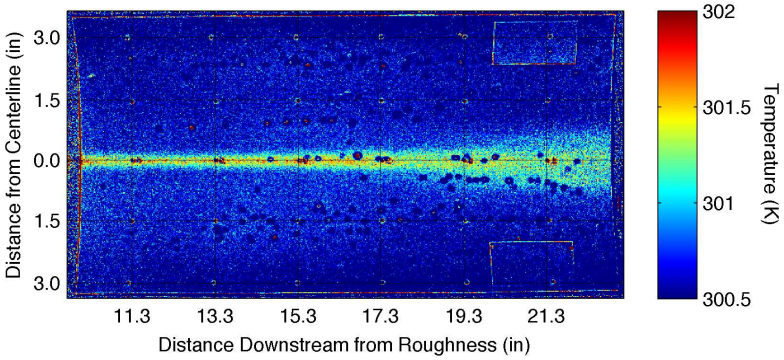

(d) $t = 2.90$ s, $P_0 = 99.3$ psia, $\frac{k}{\delta} \approx 0.55$, Re/ft $= 2.25 \times 10^6$.

Figure 19: Roughness wake temperatures when $P_{0,i} = 120$ psia, $k = 0.18$ in. Quiet flow.

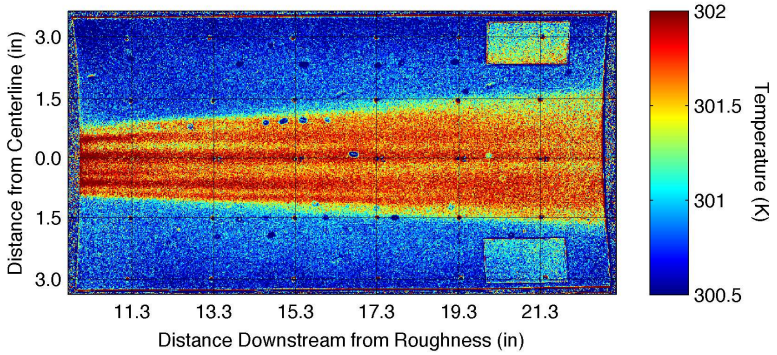

(a) $t = 1.07$ s, $P_0 = 115.6$psia, $\frac{k}{\delta} \approx 0.86$, Re/ft $= 2.62 \times 10^6$.

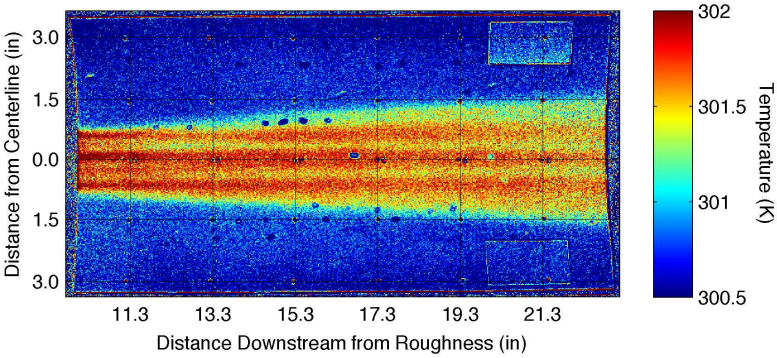

(b) $t = 1.53$ s, $P_0 = 111.1$ psia, $\frac{k}{\delta} \approx 0.84$, Re/ft $= 2.52 \times 10^6$.

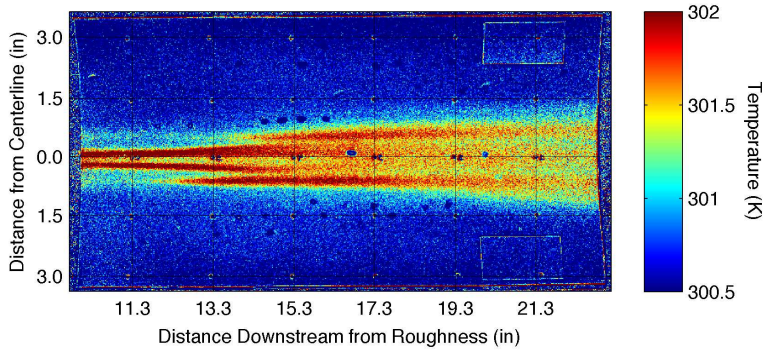

(c) $t = 2.00$ s, $P_0 = 108.5$ psia, $\frac{k}{\delta} \approx 0.83$, Re/ft $= 2.46 \times 10^6$.

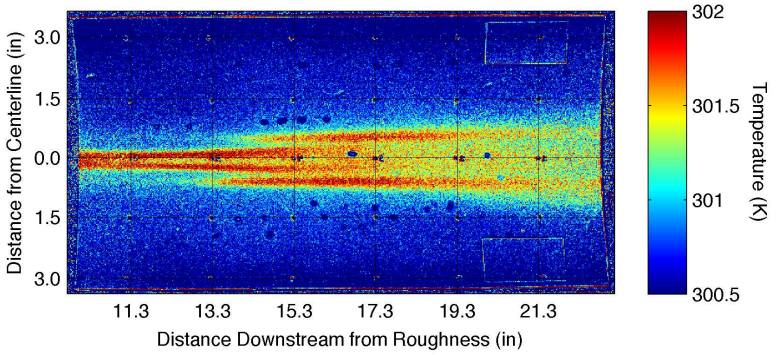

(d) $t = 2.46$ s, $P_0 = 104.4$ psia, $\frac{k}{\delta} \approx 0.82$, Re/ft $= 2.37 \times 10^6$.

Figure 20: Roughness wake temperatures when $P_{0,i} = 120$ psia and $k = 0.26$ in. Quiet flow.

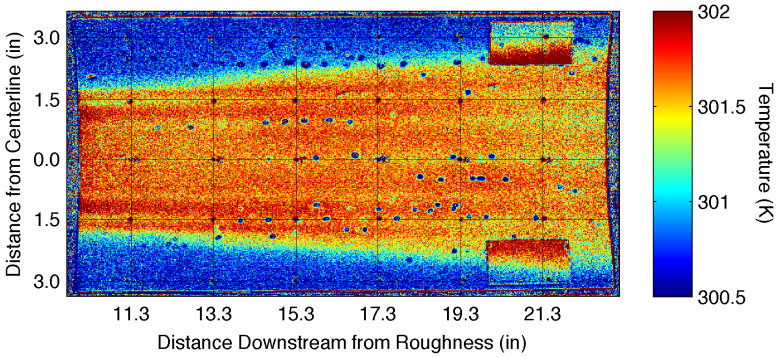

(a) $t = 1.51$ s, $P_0 = 108.4$ psia, $\frac{k}{\delta} \approx 1.27$, Re/ft $= 2.43 \times 10^6$.

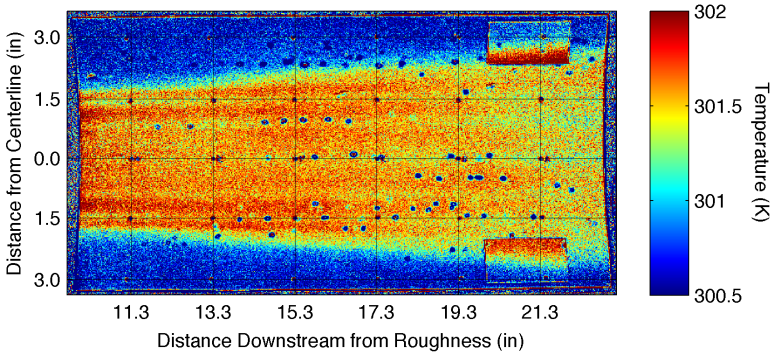

(b) $t = 1.97$ s, $P_0 = 105.8$ psia, $\frac{k}{\delta} \approx 1.26$, Re/ft $= 2.37 \times 10^6$.

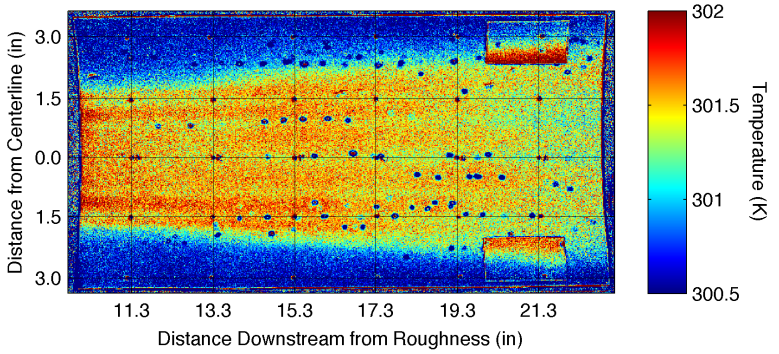

(c) $t = 2.43$ s, $P_0 = 101.8$ psia, $\frac{k}{\delta} \approx 1.23$, Re/ft $= 2.28 \times 10^6$.

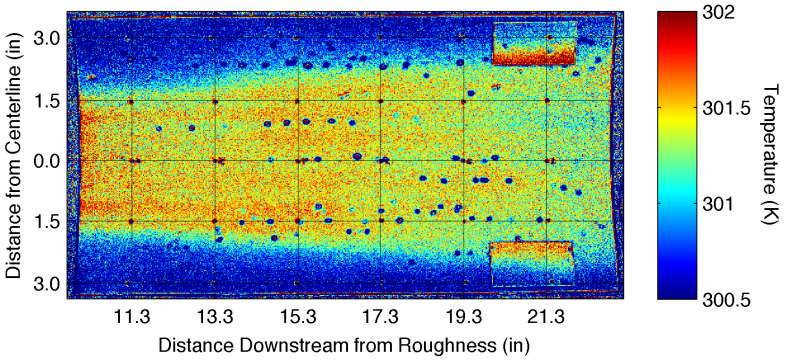

(d) $t = 2.88$ s, $P_0 = 99.4$ psia, $\frac{k}{\delta} \approx 1.22$, Re/ft $= 2.23 \times 10^6$.

Figure 21: Roughness wake temperatures when $P_{0,i} = 120$ psia and $k = 0.40$ in. Quiet flow.

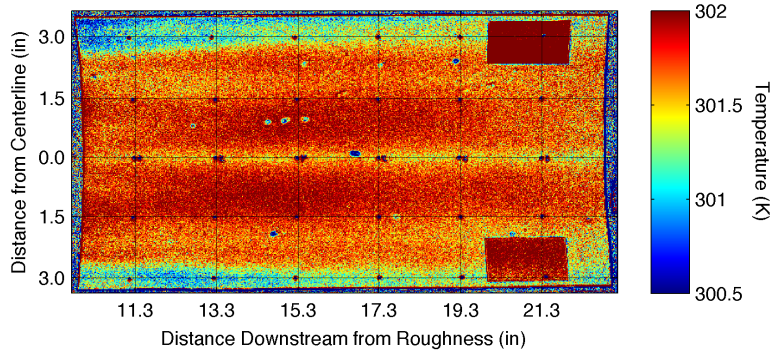

(a) $t = 1.52$ s, $P_0 = 108.7$ psia, $\frac{k}{\delta} \approx 2.42$, Re/ft $= 2.44 \times 10^6$.

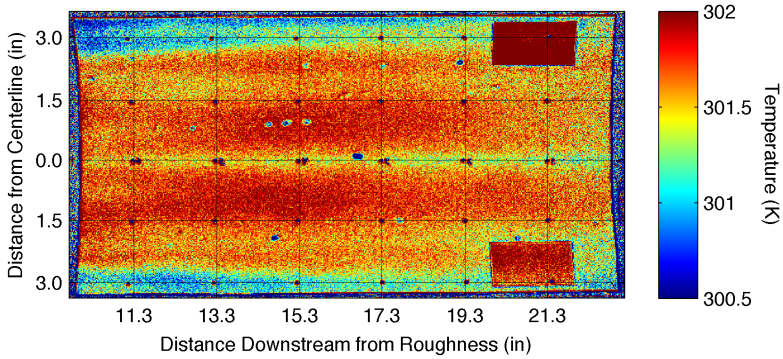

(b) $t = 1.98$ s, $P_0 = 105.9$ psia, $\frac{k}{\delta} \approx 2.39$, Re/ft $= 2.38 \times 10^6$.

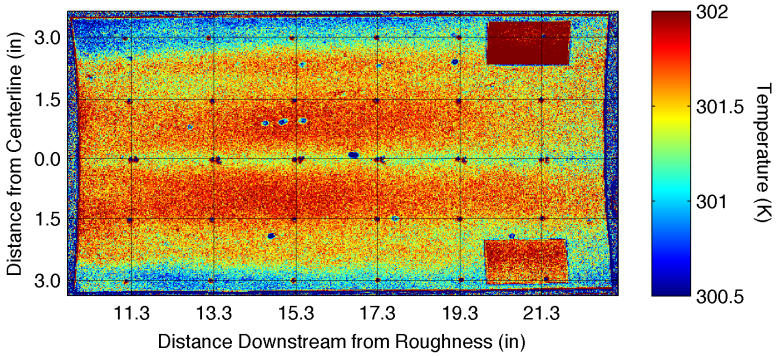

(c) $t = 2.45$ s, $P_0 = 102.0$ psia, $\frac{k}{\delta} \approx 2.35$, Re/ft $= 2.29 \times 10^6$.

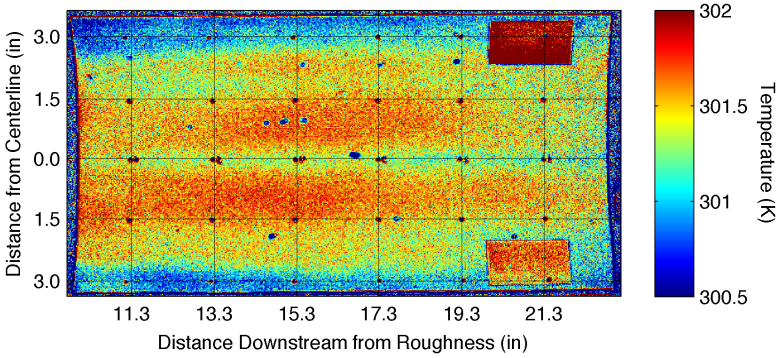

(d) $t = 2.91$ s, $P_0 = 99.3$ psia, $\frac{k}{\delta} \approx 2.32$, Re/ft $= 2.23 \times 10^6$.

Figure 22: Roughness wake temperatures when $P_{0,i} = 120$ psia and $k = 0.76$ in. Quiet flow.

References

[1]Steven P. Schneider. Effects of roughness on hypersonic boundary-layer transition. *Journal of Spacecraft and Rockets*, 45(2):193–209, March-April 2008.

[2]I. E. Beckwith and C. G. Miller III. Aerothermodynamics and transition in high-speed wind tunnels at NASA Langley. *Annual Review of Fluid Mechanics*, 22:419–439, 1990.

[3]Steven P. Schneider. Flight data for boundary-layer transition at hypersonic and supersonic speeds. *Journal of Spacecraft and Rockets*, 36(1):8–20, January-February 1999.

[4]Steven P. Schneider. Effects of high-speed tunnel noise on laminar-turbulent transition. *Journal of Spacecraft and Rockets*, 38(3):323–333, May–June 2001.

[5]M. P. Borg, S. P. Schneider, and T. J. Juliano. Effect of freestream noise on roughness-induced transition for the X-51A forebody. AIAA Paper 2008-0592, January 2008.

[6]T. Creel, I. Beckwith, and F. Chen. Transition on swept leading edges at Mach 3.5. *Journal of Aircraft*, 24(10):710–717, October 1987.

[7]T. Ito, L.A. Randall, and Steven P. Schneider. Effect of noise on roughness-induced boundary-layer transition for scramjet inlet. *Journal of Spacecraft and Rockets*, 38(5):692–698, September 2001.

[8]Steven P. Schneider. The development of hypersonic quiet tunnels. AIAA Paper 2007-4486, June 2007. Revised version to appear in the Journal of Spacecraft and Rockets.

[9]J.P. Sullivan and T. Liu. *Pressure and Temperature Sensitive Paints*. Springer, 2005.

[10]Steven P. Schneider, John P. Sullivan, Justin Rubal, Tianshu Liu, and James Crafton. Quantitative global heat transfer in a Mach-6 quiet tunnel. NASA HMMES Kickoff/TIM Presentation, April 2008.

[11]R. L. Kimmel, D. Adamczak, D. Gaitonde, A. Rougeux, and J.R. Hayes. HIFiRE-1 boundary layer transition experiment design. AIAA Paper 2007-534, January 2007.

[12]M. S. Holden T.P. Wadhams, M. G. MacLean and E. Mundy. Pre-flight ground testing of the full-scale FRESH FX-1 at fully duplicated flight conditions. AIAA Paper 2007-4488, June 2007.

[13]K. T. Berger, F.A. Greene, and R.L. Kimmel. Aerothermodynamic testing and boundary layer trip sizing of the HIFiRE flight 1 vehicle. AIAA Paper 2008-640, January 2008.

[14]Heath Johnson. HIFiRE test for Purdue tunnel. Preliminary results. Internal report, August 2007.

[15]H. B. Johnson and G. V. Candler. Hypersonic Boundary Layer Stability Analysis Using PSE-Chem. Paper 2005-5023, AIAA, June 2005.

[16]Program Development Company. *GridPro*. 300 Hamilton Avenue, Suite 409, White Plains, NY 10601, USA.

[17]M. J. Wright, G. V. Candler, and D. Bose. A Data-Parallel Line-Relaxation Method for the Navier-Stokes Equations. Paper 97-2046CP, AIAA, June 1997.

[18]I. Nompelis, T. W. Drayna, and G. V. Candler. A Parallel Unstructured Implicit Solver for Hypersonic Reacting Flow Simulation. Paper 2005-4867, AIAA, June 2005.

[19]Thomas J. Juliano, Rodrigo Segura, Matthew P. Borg, Katya M. Casper, Michael J. Hannon Jr., Brad M. Wheaton, and Steven P. Schneider. Starting issues and forward-facing cavity resonance in a hypersonic quiet tunnel. AIAA Paper 2008-3730, June 2008.

[20]Thomas J. Horvath, Scott A. Berry, and Brian R. Hollis. Boundary layer transition on slender cones in conventional and low disturbance Mach 6 wind tunnels. AIAA Paper 2002-2743, June 2002.

[21]Ndaona Chokani, Alexander N. Shiplyuk, Andrei A. Sidorenko, and Catherine B. McGinley. Comparison between a hybrid constant-current anemometer and constant-voltage anemometer in hypersonic flow. AIAA Paper 2004-2248, June 2004.

[22]C. Alba, H. Johnson, and G. Candler. Boundary layer stability calculations of the HIFiRE Flight 1 Vehicle in the LaRC 20- Inch Mach 6 Air Tunnel. AIAA Paper 2008-505, January 2008.

[23]Karen Berger. FRESH-FX Mach 6 aeroheating test update. NASA LaRC internal report, January 2007.

[24]Erick O. Swanson. *Boundary Layer Transition on Cones at Angle of Attack in a Mach-6 Quiet Tunnel*. PhD thesis, Purdue University School of Aeronautics & Astronautics, August 2008.

[25]Scott A. Berry and Thomas J. Horvath. Discrete-roughness transition for hypersonic flight vehicles. *Journal of Spacecraft and Rockets*, 45(2):216–227, March–April 2008.

[26]Jr A.H. Whitehead. Flowfield and drag characteristics of several boundary-layer tripping elements in hypersonic flow. Technical Report TN- D-5454, NASA, October 1969.